Article

Impact resistance of 3D printed discontinuous fibrous composites with Bouligand structure.

Lizhi Guan [a], Weixiang Peng [a], Rachel Ng Jing Wen [b], Jingbo Fan [b], Hortense Le Ferrand [a, b, c, *]

[a] School of Mechanical and Aerospace Engineering, Nanyang Technological University, 639798, Singapore

[b] School of Materials Science and Engineering, Nanyang Technological University of Singapore, 50 Nanyang Avenue, 639798, Singapore

[c] Singapore Centre for 3D printing, Nanyang Technological University of Singapore, 50 Nanyang Avenue, 639798, Singapore

* corresponding author. Email: hortense@ntu.edu.sg

Abstract

The Bouligand structure found in the dactyl club of the mantis shrimp is known for its impact resistance. Yet, Bouligand-inspired reinforced composites with 3D shapes and impact resistance have not yet been demonstrated. Here, direct ink writing is used to 3D print composites reinforced with glass microfibres assembled into Bouligand structures with controllable pitch angles. The energy absorption of the Bouligand composites under impact was found to surpass that of composites with unidirectional microfibre alignment. Also, the Bouligand composites with a pitch angle of 40˚ exhibited a maximum energy absorption of 2.4 KJ/m^2, which was 140 % higher than the unidirectional composites. Furthermore, the characterization of the

topography of the fractured surface supplemented with numerical simulations revealed the combination of crack twisting and crack bridging mechanisms. Flexural tests conducted on the composites with a pitch angle of 40˚ also showed maximum properties, with a flexural strength of 36.9 MPa, a stiffness of 2.26 GPa, and energy absorption of 8 KJ/m^2. These findings are promising for the microstructural design of engineered composites using direct ink writing for applications in aerospace, transportation, defence, etc.

1. Introduction

Microstructural design in reinforced composites significantly influences their mechanical properties, particularly their resistance to catastrophic failure. Researchers have been inspired by the microstructures found in biological materials to create artificial composites with strength and toughness.[1] One remarkable biological composite is the dactyl club of the mantis shrimp, which can withstand impact and cavitations forces up to 1501 and 504 N, respectively.[2] Previous studies reported that the periodic region in the dactyl club contributed most to its impact resistance, thanks to the helicoidal arrangement of mineral nanorods in a so-called Bouligand structure.[3] In this structure, layers of aligned mineral nanorods are stacked on top of each other but with a small angle turn between each adjacent layer.[3] This angle, the pitch angle, provides the Bouligand structure shear wave filtering effect and enhances its energy absorption upon fracture.[4] Synthetic composites with Bouligand structures have shown promising results. For example, Bouligand cement composites reinforced with discontinuous steel fibres of ~12 mm length have shown toughness under drop-weight impacts, thanks to mixed modes of fracture

with crack deflection, twisting, branching, bridging and micro-cracking.[5] Bouligand composites reinforced with continuous glass fibres tested under Charpy impact revealed an increase in energy absorption attributed to crack-twisting,[6] while under quasi-static fracture, they exhibited a combination of crack twisting and crack bridging.[7] However, to the best of the author's knowledge, the impact resistance mechanisms in Bouligand composites have not being investigated in notched samples. Also, microfibre reinforced composites with Bouligand structure, 3D shapes, and impact resistance, are still to be demonstrated.

To create Bouligand composites, one strategy consists in manually laying-up long fibre reinforced polymer laminates with a controlled angle between each layer.[8-10] However, the use of continuous long fibres poses drastic constraints on the shapes. In contrast, the use of short fibres allows the creation of liquid inks or pastes that can be used in additive manufacturing processes. For instance, Bouligand composites have been produced by brush-induced assembly of short micro/nanofibers on a heated substrate.[11] In other works, adjusting the pH, aspect ratio and concentration of chitin whiskers in a solution could trigger their self-assembly into a Bouligand structure.[12] However, these strategies still face limitations in terms of scalability, control of the Bouligand pitch angle, freedom to achieve complex 3D shapes and overall efficiency. Having a fabrication method that can tailor the structural parameters, such as the pitch angle, would allow rational design and optimisation of the Bouligand structure for high impact resistance in fibre reinforced composites.

To enable such rational structural design, an efficient fabrication approach is 3D printing. To align microfibers at any desired angles, 3D printing has been combined with external fields.[13] For example, stereolithographic 3D printing has been combined with electric fields to align carbon

nanotubes (CNTs) within each deposited layer.[14] However, stereolithography requires a liquid resin that cures using UV which limits the loading in CNTs and the mechanical properties. In turn, extrusion-based 3D printing techniques such as fused deposition modelling (FDM) and direct ink writing (DIW) do not have these limitations. FDM melts, extrudes, and deposits thermoplastic filaments on a cool substrate, whereas DIW pushes viscous inks with shear-thinning and thixotropic properties through a nozzle on a substrate. Because of the extrusion at the nozzle in both methods, shear can cause alignment of microfibers distributed in the filaments or in the ink, along the printing direction.[15] To form Bouligand structures, it therefore suffices to control the direction in which the nozzle is moving in each layer to set the orientation of microfibers present in the extruded material.[14] Using FDM, Bouligand structures have been made, showing improvement on their specific impact energy.[6] However, delamination of the composite occurred during failure, likely due to the inevitable voids between the extruded lines that resulted in weak interfaces. In addition, FDM also has constraints on the achievable fibre concentration and thus on the achievable mechanical properties. These are serious issues for future practical and commercial applications. In turn, DIW has been shown of being capable of 3D printing a wide diversity of compositions, including viscous inks with high concentrations in reinforcing particles.[16] Using DIW to 3D print Bouligand structures could therefore potentially overcome the limitations of FDM and achieve higher mechanical properties, while enabling fine control over the microstructure to test and understand the energy-dissipating mechanisms during fracture.

In this work, epoxy composites reinforced with glass microfibers assembled into Bouligand structures with controllable pitch angle are 3D printed using DIW and their impact resistance and

flexural properties are tested. Numerical simulations are conducted to support the experimental results to study the fracture mechanisms. First, the rheological properties of a viscous ink containing glass microfibers are optimized to yield an ink printable using DIW and allowing alignment of the glass microfibers along the printing direction. Subsequently, Izod impact tests are conducted on notched 3D printed composites to compare the energy absorption of unidirectional and Bouligand structures. The fractured specimens are inspected using scanning electron microscopy (SEM), laser microscopy, and micro computed tomography (micro-CT), which allow the characterisation of the surface morphology, porosity and cracking mechanisms. The flexural properties of the composites are also tested to compare the dynamic with the quasi-static fracture behaviours. The findings from this study provide insights to 3D print lightweight impact resistant reinforced composites, for potential applications in aerospace, automotive industry, and defence, among others.

2. Materials and Methods

2.1. Materials

Carbon black was obtained from PRINTEX® XE 2-B and multi-walled CNTs (MWCNTs) were obtained from Graphistrength® Arkena Innovative Chemistry. E-Glass fibers which were milled glass microfibres were sourced from Japan's Nippon Electric Glass Co. Their length and diameter microfibers ranged 20-300 µm and 7-14 µm, respectively, with an average of 50 µm and 10 µm (see Supplementary Information (SI) Figure S1). Commercial epoxy resin and epoxy hardener (Casting Resin MS1000) were purchased from WEICON South East Asia Pte Ltd.

2.2. Methods

2.2.1. Ink preparation

MWCNTs (0.15 g) and carbon black (0.03 g) were dispersed into 7.98 g of epoxy resin using Thinky Mixer (THINKY ARE-250, Japan) for 5 minutes at 2000 rpm. Subsequently, the glass microfibres (5.25 g) were added to the above mixture and mixed for 5 minutes at 1000 rpm using an overhead mixer (Base Hei-TORQUE VALUE 400, Heidoph Instruments GmbH & Co. KG, Germany). Following this, 1.59 g of epoxy harder was introduced and mixed using the same overhead mixer for 5 minutes at 500 rpm at cold temperature (in an ice bath). The slow speed of the mixing and the use of the ice bath reduced the heat generated from the mixing and slowed down the epoxy reaction and the consolidation of the mixture which is the ink for DIW.

2.2.2. DIW of Bouligand composites

The 3D printing set-up (3D Potter Micro 8, 3D Potter Inc. USA) consisted of a vertical nozzle with a mechanical piston to extrude the ink through the nozzle. The 3D models were created using a computer-aided design software (Rhinoceros 7). IdeaMaker was used to slice the designs into layers for the printing. Unidirectional microfibers orientation at angles $\alpha = 0°$, 45°, and 90° within one layer, and Bouligand structures with various pitch angles $\gamma = 10°$, 20°, 40°, 60°, and 90° were designed. The following printing parameters were used: diameter nozzle of 0.8 mm, printing speed of 8 mm/s, layer thickness of 0.4 mm, flow rate of 50%. At least six specimens of each design were printed for each test. The dimensions of the printed specimens (length, width, and depth) are 64 mm, 6 mm and 12.8 mm. For these dimensions, 34 layers were deposited on

top of each other. Since the number of total layers is fixed, but the pitch angle is varied, the period of the helicoidal assembly decreases as the pitch angle increases following:

$$\text{period} = \frac{34*\gamma}{180}. \quad (1)$$

Therefore, the periods of the Bouligand structures with γ = 10°, 20°, 40°, 60°, and 90° are 1.8, 4, 7.5, 11.3 and 16.5, respectively (see SI Figure S2 for the schematics of the 3D printed structures).

2.2.3. Impact tests and characterisation.

Izod impact tests were conducted using the Tinius Olsen impact machine (Willow Grove, PA, U.S.A.) following the ASTM standard D256. A V-notch of 2 mm depth was cut using a sample notcher (DS-93). The size of the impacted samples was: 64 mm (length, l), 12 mm (width, b_N) and 4 mm (thickness, h). The applied pendular energy was 3.3669 J. The impact speed rate was 2.3 m/s. See SI Figure S3 for a schematic of the set-up. The impact energy absorption E_a expressed in kJ/m^2 was calculated using:

$$E_a = \frac{E_c}{h \cdot b} \times 10^3, \quad (2)$$

where E_c is the corrected energy absorbed by the specimen (in Joules); h is the thickness of the specimen (in mm); b is the remaining width (in mm) of the specimen after testing. The specimens were polished using SiC papers before impact testing.

The methods used for the other characterisations are described in the SI.

2.2.4. Finite Element Modelling

Finite element (FE) analysis was conducted using Abaqus 2020 (see Supplementary Text in SI for more details). The model was composed of the glass microfibers (length: 25 μm, diameter: 5 μm, aspect ratio: 5) assembled into Bouligand structures with the desired pitch angles γ, and surrounded by a matrix meshed with solid elements C3D4. The fibre-matrix interface was simulated with the cohesive elements. The simulated samples had representative geometric dimensions of 325 μm × 810 μm × 214 μm (length × width × depth). The volume content of microfibers (20 vol.%) used in numerical simulation was the same in the experiment. All the material properties used in the simulations are listed in Tables S1 and S2. The tensile stress-strain response of the pure matrix without glass microfibres was measured experimentally (see SI Figure S4).

3. Results

3.1. DIW of Bouligand composites.

To enable the design and fabrication of the Bouligand composites using 3D printing, the concentration of glass microfibers in the epoxy resin had to be adjusted to ensure printability (**Figure 1**). The ink is indeed required to have a high viscosity and a high yield stress to allow extrusion and shape-retention, respectively, and the possibility to print multiple layers without the collapse of the structure.[17] Glass microfibers of 50 μm width and 10 μm diameter on average were used for the reinforcements. These glass microfibers are similar in chemistry to those used in continuous long fibre composites, but the short size is necessary to permit the creation of complex shapes with good resolution *via* 3D printing. The dimensions of the microfibers is

important since they are bearing a significant percentage of the applied load.[18] Here, the aspect ratio of the microfibers ranges from 2 to 30 with an average value of 5 (**Figure 1a**). To meet the rheological requirements for DIW, carbon black and MWCNTs were introduced in the ink following a previous recipe.[19] These additional nanomaterials could also enhance the final mechanical performance, although this is not the focus of this study. The ink was optimized to enable homogeneous dispersion of the constituents and removal of the air bubbles as efficiently as possible. The finalized optimized ink contained 35 wt% of glass microfibers and had a viscosity at rest of 1000 Pa·s and a yield stress of 500 Pa (see SI Figure S5 for the rheological data), which allowed 3D printing. After the ink was mixed, it was immediately transferred into the 3D printing syringe before the epoxy matrix cured (see SI Figure S5 for the viscosity of the resin as a function of time). In practice, the curing reaction could be slowed down by using an epoxy matrix that crosslinks upon application of an external trigger such as temperature. For the aim of this study, which was to understand the mechanisms and the extent of impact resistance due to the Bouligand structure, the resin and its curing time were chosen arbitrarily. During DIW, the glass microfibres transitioned from random orientation behind then nozzle tip (**Figure 1b (i)**) to aligned orientation along the walls of the nozzle at the tip (**Figure 1b (ii)**).[15] After extrusion and deposition, the microfibres maintained their aligned orientation which was further fixed by the increase in viscosity due to the curing of the resin (**Figure 1b (iii)**). This orientation of the microfibers after 3D printing was verified by optical microscopy (**Figure 1c** and SI Figure S6).[20] The precise alignment of glass microfibers can therefore be combined with complex 3D shapes (**Figure 1d**). The 3D microstructure in printed parts of complex shapes can be resolved using micro-CT (see SI Video S1 for the micro-CT scan of a Bouligand structure with a pitch angle of 90˚). After curing,

the printed reinforced composites retained their shape and microstructure, and had a low density of 1.4 g/ml.

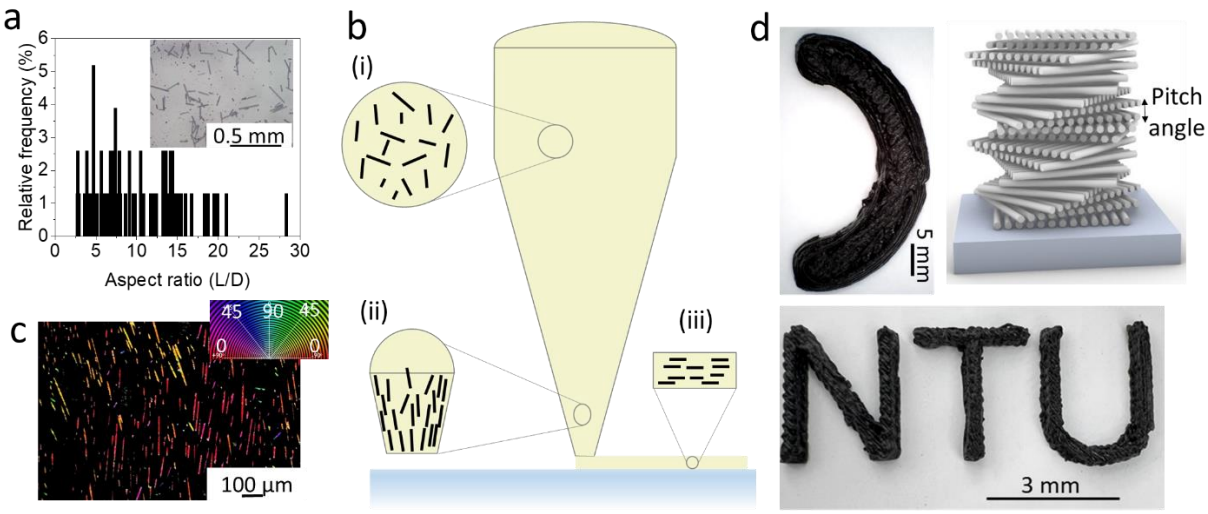

Figure 1. DIW of glass microfiber reinforced epoxy composites with Bouligand structure. **(a)** Distribution of the aspect ratios of the glass microfibers used for the ink preparation. Inset is an optical image of the glass microfibers**. (b)** Illustration showing the orientation of the microfibres at different positions during the 3D printing: (i) disordered distribution behind the nozzle tip; (ii) alignment near the tip by shear forces; (iii) aligned orientation in the 3D printed part. **(c)** Microscopic image of the glass microfibers in an extruded layer juxtaposed with its hue-saturation-brightness (HSB) color-coded map which shows the angles of the microfibres in the image. **(d)** Intricate 3D printed shapes with a Bouligand structure and schematics of this structure.

3.2. Impact energy absorption

The control of the microstructure during 3D printing is convenient to study the effects of the microstructural design on the impact resistance.[21] First, we designed and fabricated composites with unidirectional microfibre orientations (**Figure 2**). To observe the effect of fibre orientation on the crack propagation, the composites were purposely printed and tested at various microfibre angles α with respect to the impacting direction (e.g., α = 0˚ was for microfibres parallel to the impacting direction). Composites with microfibres oriented at α = 0°, 45°, and 90° were successfully 3D printed, notched, and submitted to impact Izod test (**Figure 2a**). As shown in **Figure 2b**, the energy absorption of all unidirectional composites was higher than that of the control composite without any glass microfibre. Increasing α increased the impact energy absorption of the composites from 0.514 KJ/m^2 for α = 0˚ up to 1.1 KJ/m^2 for α = 90˚. To explore the toughening mechanisms, the morphology of the fractured surface was captured for each microstructure (**Figure 2c-f)**. The control composites presented a straight crack along the notched direction. Addition of microfibers with α = 0˚ orientation showed also a very straight crack along the notched direction which was parallel to the microfibres. From the electron micrographs in **Figure 2d**, crack slippage along the microfibres resulted in river-like structures with hackles and ribbons at the fractured surface which contributed to increasing the energy absorption as compared to the control composites. These types of white marks are typical of ductile deformation of the matrix by the presence of reinforcements.[22] Because there is no increase in crack tortuosity between the control composites and the composites with α = 0˚, the difference in energy absorption is negligible. However, increasing of the orientation angle to α = 45˚ deviated the crack from the notch direction following the microfibres orientations, extending

the crack length and leading to increased energy absorption. Additionally, it can be observed that some of glass microfibres were pulled out from the matrix (red arrows in **Figure 2e)**. This phenomenon, along with the crack slippage, contributed to a higher energy absorption in comparison to the composites with $\alpha = 0^{\circ}$. Increasing further the orientation angle to $\alpha = 90^{\circ}$, the fractured surface morphology appeared rougher. Electron micrographs showed that most microfibres got pulled out and broke during the impact, indicating crack bridging mechanism (**Figure 2f**). Crack deflection led to more tortuosity and the presence of microfibres perpendicular to the notch direction and therefore perpendicular to the crack propagation direction, increased the energy dissipation. Overall, these series of experiments give insights on the modes of fracture propagation in our microfibre reinforced composites. At angles below 45°, the crack tends to propagate along the microfibres with mediocre increase in the total energy absorption. Increasing the orientation angle to 90° results in a greater degree of crack deflection and energy absorption with fracture of the microfibres. From $\alpha = 0^{\circ}$ to 90°, a transition between two fracture mechanisms is observed with slippage at low angles and fibre pull-out at higher angles. Furthermore, there is some correlation between an increased impact energy absorption and a higher surface roughness. How the surface morphology and topography reflect the failure behaviour has indeed been reported in a number of studies.[23-25] Therefore, tailoring the microstructure to significantly enhance the surface roughness can be expected to further amplify the energy absorption during fracture. We verify this hypothesis next in composites with 3D printed Bouligand structure having $\alpha = 90^{\circ}$.

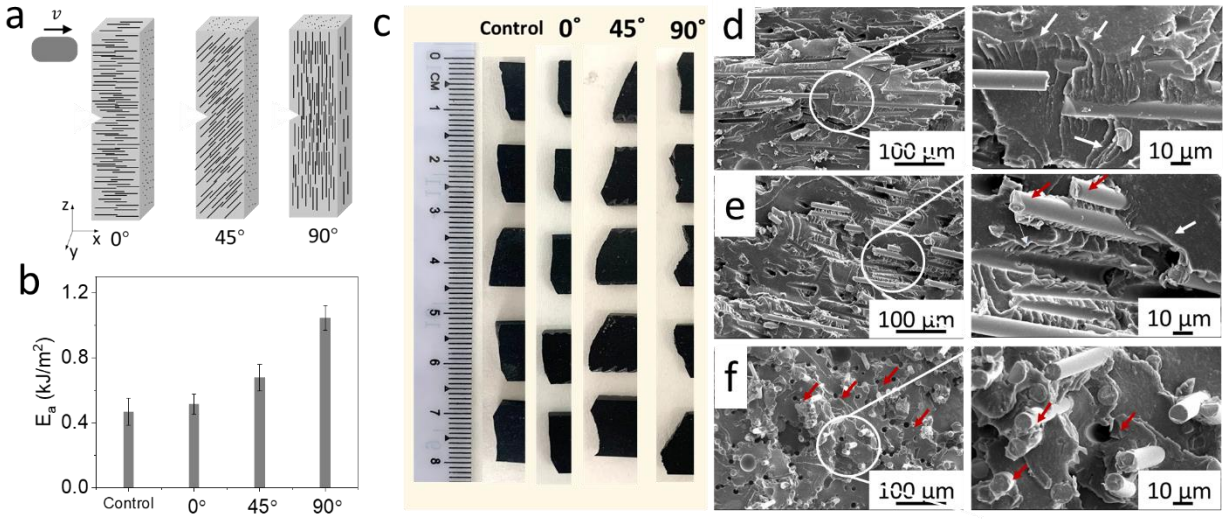

Figure 2. **Impact tests on composites with unidirectional microfibre orientations at 0°, 45°, and 90°. (a)** Cartoons showing the microstructure of composites with microfibres oriented at angles of α = 0, 45 and 90° prepared for Izod impact test. **(b)** Energy absorption E_a for control composites (no microfibres) and reinforced composites with increasing angle α. **(c)** Pictures of the fractured composites after the impact tests. Electron micrographs of the composites with unidirectional orientation at **(d)** α = 0°, **(e)** α = 45°, and **(f)** α = 90°. White arrows indicate river-like structures with hackles and ribbons. Red arrows indicate the pull-out and breakage of the glass microfibres.

To demonstrate that Bouligand microstructure can indeed create rough fractured surfaces and increase the energy absorption, we 3D printed composites with pitch angles of γ = 0˚, 10˚, 20˚, 40˚, 60˚ and 90˚ (**Figure 3)**. Conducting the same impact tests as for unidirectional composites, higher energy absorption was indeed recorded for all pitch angles (**Figure 3a)**. The minimum energy absorption of the Bouligand composites was obtained at γ = 10˚ with a value of

1.5 KJ/m^2. Increasing the pitch angle to γ = 40˚, a maximum energy absorption of 2.48 KJ/m^2 was obtained. Past γ = 40˚, the composites exhibited lower impact resistance down to 1.6 KJ/m^2 at γ = 90˚. The excellent energy absorption of the Bouligand composites as compared to the unidirectional ones was attributed to the Bouligand structure and revealed that there is an optimum pitch angle at which the energy absorption is maximum. 40˚ seems to give the best properties for our composites. This is different from Bouligand structures made from other materials which showed a maximum toughness for a much lower pitch angle of about 9.47˚.[6] This is likely due to the difference in chemical composition and microfibre size. Indeed, it has been reported that the aspect ratio of the microfibre drastically modifies the response of composites.[7] To better understand the performance of our Bouligand composites and to verify the importance of the pitch angle, we analysed more carefully the fractured surfaces. More precisely, we measured the surface topography of the fractured surfaces and quantified the surface arithmetical mean roughness Sa and the developed interfacial area ratio Sdr. As depicted in **Figure 3b**, increasing the pitch angle increased Sa and Sdr from 180 µm and 1.3, respectively, at γ = 10˚, to the maximum values of 600 µm and 1.9, respectively, at γ = 40˚. At higher pitch angles, Sa and Sdr decreased again, down to 190 µm and 1.4, respectively, at γ = 90˚. Interestingly, the impact energy absorption E_a was found to vary exponentially with Sa with a coefficient of correlation $R^2 = 0.99$ (**Figure 3c**). Such exponential correlation between roughness and energy absorption is analogous to the exponential correlation between roughness and flexural toughness reported elsewhere.[23] Furthermore, the morphologies of the entire fractured surfaces were also obtained through reconstructed 3D views (**Figure 3d-h**). In the Bouligand composites with γ = 10˚ (**Figure 3d**), the fractured surface was relatively smooth, and the crack slipped along

the microfibres (see SI Figure S7 for electron micrographs of the fractured surfaces), which indicated crack twisting as the dominant fracture mechanism. The fracture surface of the composites with γ = 20˚ displayed two “mountain-like” features that were the result from crack deflections along the microfibers orientations. The peaks of the "mountains" likely correspond to the areas where the microfibers were at 90˚. Although within the scanned area, there were four periods of the structure and it can be expected that the microfibres were at 90˚ four times, only two "mountain-like" features were observed. One probable reason for this discrepancy is that the fracture of composites is a complex process that cannot be predicted with 100% accuracy, particularly in our composites where defects like bubbles and misalignments are present. Nevertheless, the trends observed experimentally correlate well with the microstructures. Apart from the two "mountain-like" regions, the rest of the fractured surface was relatively smooth (see SI Figure S7 for electron micrographs of the fractured surface). As the pitch angle increased further to γ = 40˚, the surface roughness of the fracture surface increased with more fracture of the microfibres and large crack deflection events. Beyond γ = 40˚, the topographies of the fractured surfaces appeared smoother with more continuous crack paths (**Figures 3g and h)**. Overall, the cracking mechanisms in the Bouligand composites include crack twisting and crack bridging. When both mechanisms happened, the fractured surface area is amplified, resulting in higher energy absorption. The transition from predominantly crack twisting mode at small pitch angles to predominantly crack bridging mode at high pitch angles has also been reported in other works, although at smaller pitch angles as discussed previously.[7] Our results demonstrate that by carefully tuning the pitch angle thanks to 3D printing, it is possible to tailor the fractured surface roughness to achieve a maximum energy absorption. This enhancement in the impact resistance

comes despite the presence of defects like gaps, bubbles and misalignment that cannot be avoided. We measured indeed a small amount of porosity in our composites (**Figure 3i**), which may also contribute positively to the energy absorption.[6] Overall, the impact resistance achieved in our 3D printed Bouligand composites is therefore quite remarkable.

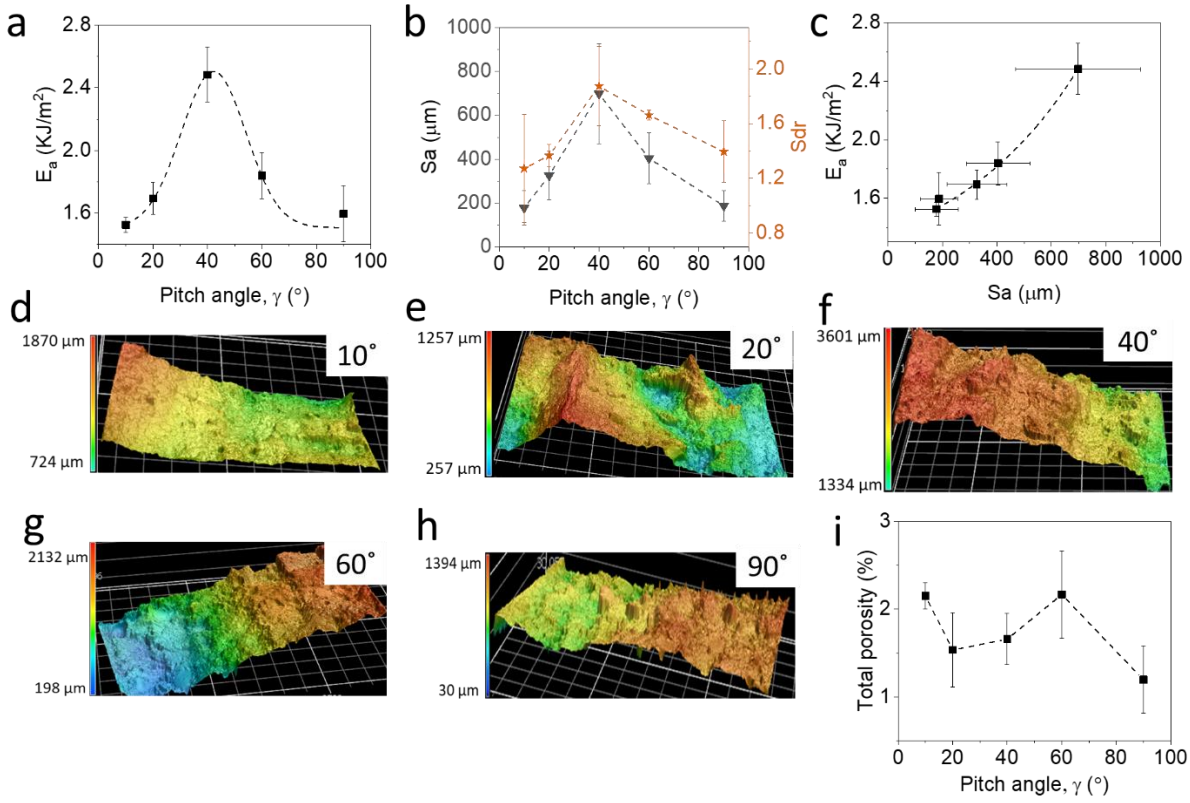

Figure 3. Impact performance of the Bouligand composites at various pitch angles. (a) Impact energy absorption and **(b)** the fractured surface roughness of the composites with Bouligand structure as a function of the pitch angle γ. Dotted lines are guides to the eye. **(c)** Energy absorption as a function of the surface roughness. The dotted line is an exponential fit with coefficient of correlation $R^2 = 0.99$. **(d-h)** Topographies of fractured surface of the Bouligand

composites for each pitch angle. For all images, the fracture propagated from the left to the right.

(i) Total porosity of the composites as a function of the pitch angle.

The Bouligand composites with a pitch angle of 40˚ exhibited highest energy absorption during impact. Closer look at the topography of the fracture surface further confirmed the fracture mechanisms discussed above (**Figure 4**). High crack tortuosity along the impact direction (in the XZ plane) likely results from the combination of crack twisting and crack bridging (green colour in **Figure 4a**). The straight crack path in the YZ plane at the back of the composite (orange colour) suggests that the crack propagated along the direction of the microfibres within each aligned layer. From the electron micrographs in **Figure 4b**, two regions can be highlighted. The top region framed by the red dotted lines presenta smooth fracture surface topography because the crack propagated along the microfibres orientation. This is confirmed with the image at higher resolution in **Figure 4c**. In turn, the bottom region framed by the white dotted lines shows relatively rough surface topography and a lot of glass microfibres pulled out and broken which are also confirmed at higher resolution (**Figure 4d**). The combined crack twisting and bridging mechanisms therefore contribute to the high impact energy absorption in Bouligand composites with pitch angle of 40˚.

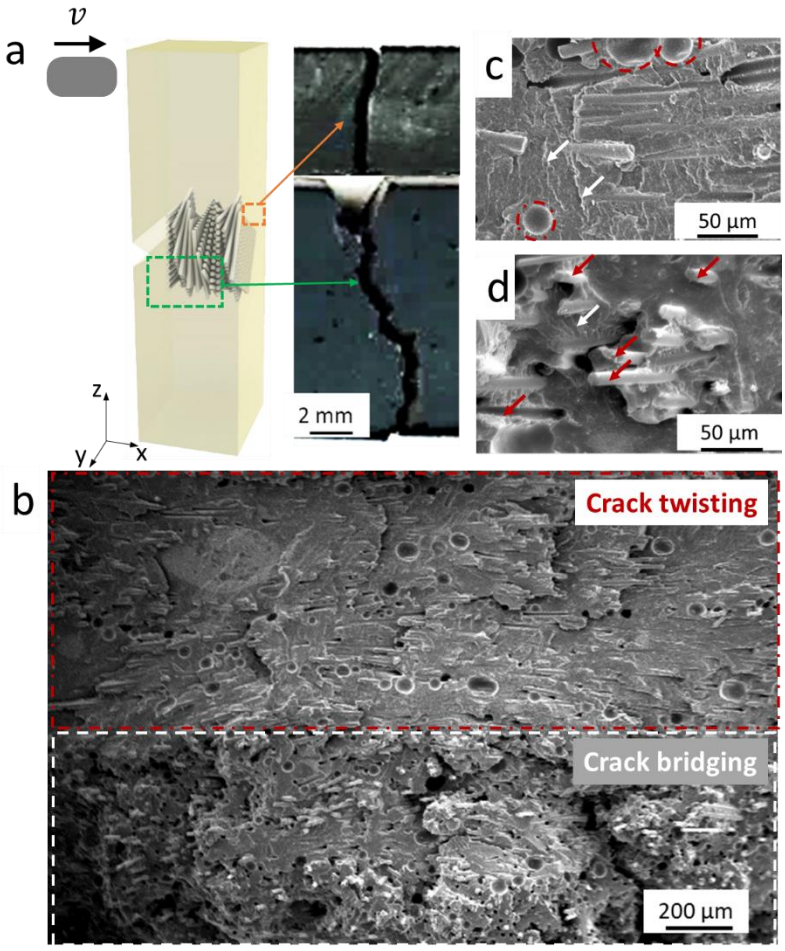

Figure 4. The fractured morphology of the Bouligand composites with a pitch angle of 40˚. (a) Cartoon and images of the fractured specimen in the XZ plane (green colour) and in the YZ plane (orange colour); **(b)** Electron micrograph of fractured surface showing crack twisting and crack bridging regions and zoomed-in micrographs in (**c)** and **(d)**, respectively. The red circles indicate micro voids, the red arrows indicate broken microfibres and the white arrows indicate the cracks in the epoxy matrix.

3.3. Numerical simulation analysis

To confirm the experimental results, numerical simulations were conducted using the finite element method (**Figure 5**, see SI Figure S8-S10 and supplementary text for details about the simulations).[26] The mechanical properties of the matrix were obtained experimentally (see SI Table S1), whereas the interfacial properties between the fibre and the matrix were modelled with cohesive elements (see SI supplementary text and Figures S8-10). The simulation of the impact tests of the Bouligand composites with pitch angles from 10˚ to 90˚ reveals a maximum energy absorption at 40˚, which confirms the experimental results (**Figure 5a**). Interestingly, the energy absorption of the Bouligand composites increases with the impact speed, while the maximum value is still obtained at the pitch angle of 40˚ for all speeds. This suggests that the impact speed does not affect the optimum pitch angle. Likewise, the use of a matrix with a higher mechanical strength and the increase in impact speed can increase the energy absorption values but does not change the optimum pitch angle (see SI, Table S2 and Figure S11 for simulations with higher strength matrix). After impact failure, the fracture morphologies present similar crack propagation features as in the experiments. In Bouligand structures with γ of 10˚, the crack propagated along the microfibres, revealing crack twisting as the dominant fracture mode **(Figure 5b**). Increasing γ to 40˚, crack twisting along the microfibres orientation and crack bridging are observed (**Figure 5c**). In the Bouligand structure with γ of 90˚, the crack twisted when the microfibres were parallel to the notch direction, while crack bridging occurred when the microfibres are perpendicular to the notch direction (**Figure 5d)**. Therefore, we can confirm the transition from crack twisting to crack bridging at the optimum pitch angle of 40˚. In addition, the numerical simulations also provide information on how the composites fracture during the

impact. **Figure 5e** and SI, Video S2 illustrate the entire failure under impact for the Bouligand composite with γ = 40˚. Before impact, the sample was relaxed and there was no stress observed at its surface. Once the pendulum strikes, stresses quickly accumulated at the notch tip (red arrow) and at the opposite region near the clamp holder (black arrow). These stress concentrations led to cracking at these regions which then propagated and eventually met each other.

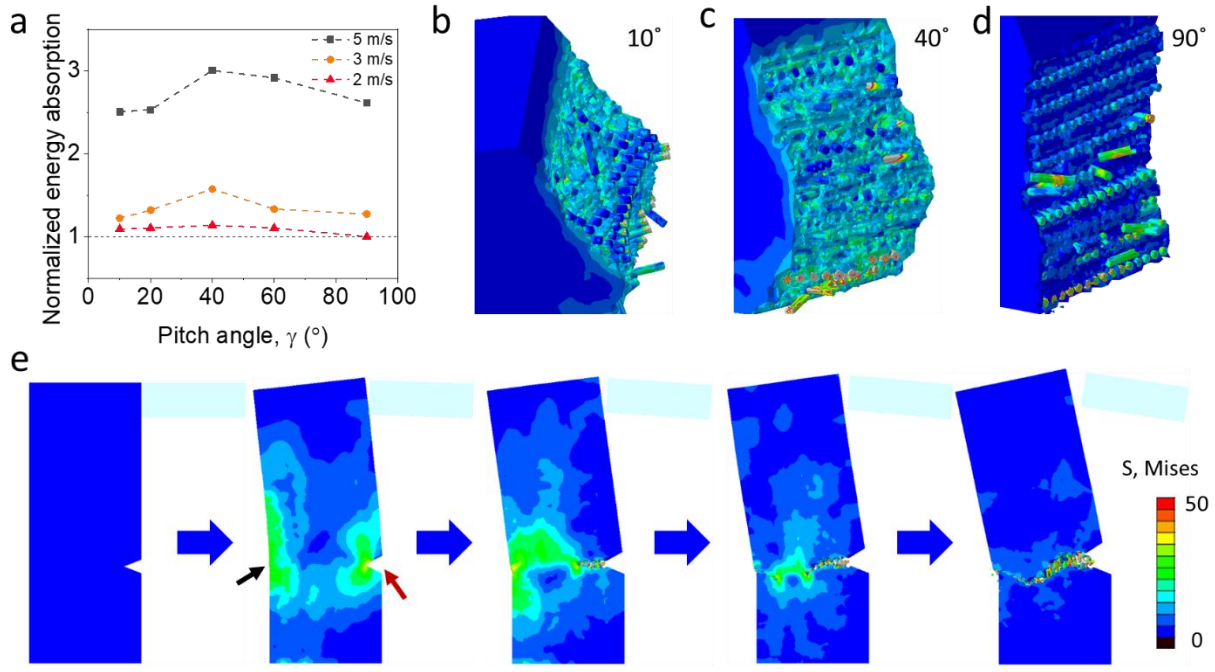

Figure 5. Simulation of the fracture of the Bouligand composites under impact. (a) Energy absorption of Bouligand composites normalized by the energy absorption of the composites at γ = 90˚, as a function of the pitch angle under impacts at different speed (2 m/s, 3 m/s and 5 m/s). Fracture morphologies of the fractured Bouligand composites with γ of **(b)** 10˚, **(c)** 40˚, and **(d)** 90˚. **(e)** Snapshots showing the fracture of the Bouligand composite with γ = 40˚ under impact from the top right corner (impactor represented by the light blue area). The colour code

represents the local tensile stresses. The black arrow near the clamp holder and red arrow at notch tip indicated the stress concentration and crack initiation.

3.4. Quasi-static bending test

The simulated results pointed out that the little effect of the impact speed on the optimum pitch angle. This point is important since in practical applications, the composites undergo various types of loadings. Furthermore, other studies tested the quasi-static fracture of Bouligand composites of other composition. Therefore, we performed 3-point bending tests to estimate the flexural performance of our Bouligand composites at various pitch angles (**Figure 6a**). All composites exhibited a flexural strength between 20 and 40 MPa and a flexural modulus between 1.6 and 2.4 GPa which are relatively high strength and modulus for 3D printed fibre reinforced polymers (**Figure 6b**).[27] These values could be optimized by choosing a stronger resin or other constituents in the ink. More interestingly, again, the Bouligand composites with a pitch angle of 40˚ exhibited the maximum flexural strength and modulus, with values of 37 MPa and 2.26 GPa, respectively. These values show an enhancement by 48% and 28% as compared to the composites with a pitch angle of 10˚ and 90˚, respectively. In turn, Bouligand composites with a pitch angle smaller than 40˚ exhibited a higher strain at fracture. For instance, the composites with a pitch angle of 10˚ broke at 4% strain, whereas composites with a pitch angle of 90˚ broke at 2% strain (**Figure 6c**). The composites with small pitch angles show crack twisting and large fractured surface area resulting in larger strains at failure, whereas composites with high pitch angles show crack bridging and straight cracks, resulting in lower flexural strains at failure.

Furthermore, calculation of the flexural energy absorption E_s by integrating the force-displacement curves gives an estimation of the quasi-static toughness of the composites. When plotting E_s as a function of the pitch angle, 40˚ is still the pitch angle yielding the highest value (**Figure 6d)**. E_s increased linearly from γ = 10˚ to 40˚, reaching a maximum value of 8 KJ/m^2 at γ = 40˚. However, past 40˚ pitch angle, E_s largely decreased down to 4 KJ/m^2 at γ = 90˚. Finally, the crack path in the Bouligand composites with γ = 40˚ showed high tortuosity which likely contributed mostly to the energy absorption during testing (**Figure 6e**). Electron micrographs of the fractured surface also displayed the combined fracture mechanisms with crack twisting and crack bridging (**Figure 6f)**. These results confirm the little influence of impact speed as in the simulations.

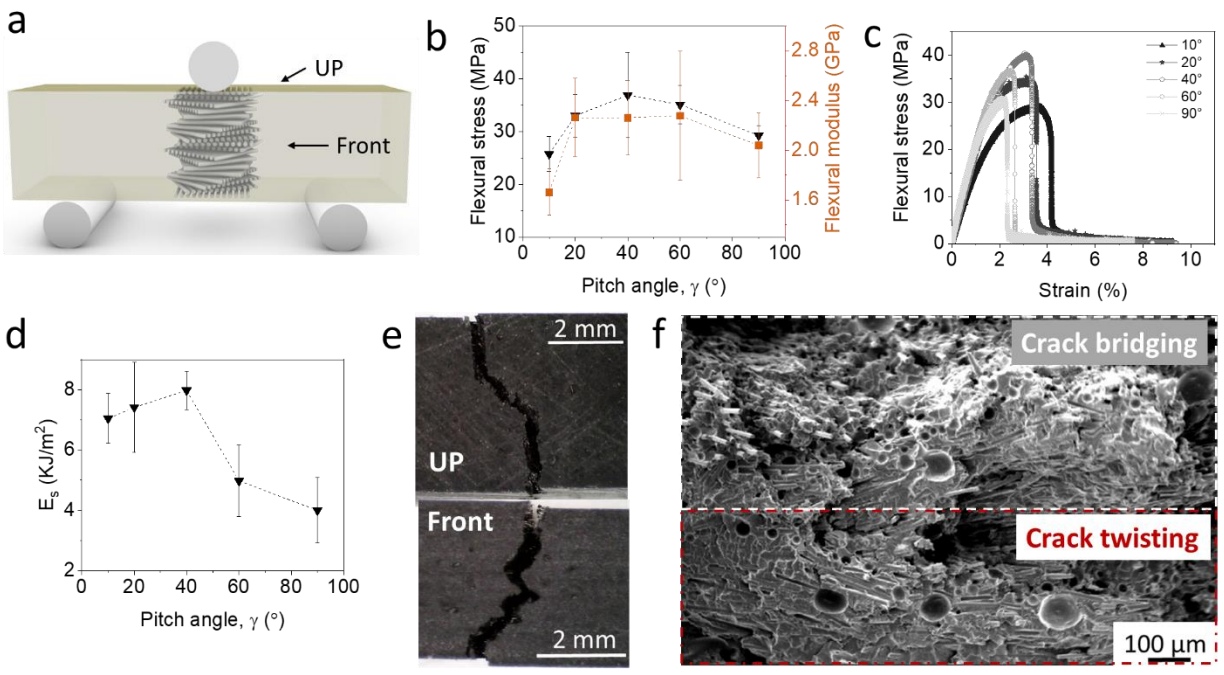

Figure 6. Flexural properties of the Bouligand composites as a function of the pitch angle. (a) Schematic of three-point bending test on the Bouligand composites. **(b)** Flexural strength (black)

and modulus (orange) as a function of the pitch angle. **(c)** Representative stress-strain curves recorded during the flexural test for Bouligand composites of different pitch angle. **(d)** Flexural energy absorption E_S of the composites as function of the pitch angle. The fractured morphology of the composites with a pitch angle of 40˚: **(e)** optical pictures and **(f)** electron micrograph.

4. Discussion

In this work, we 3D printed discontinuous glass microfiber composites with controlled microstructures using DIW. The composites with unidirectional orientation possess a maximum energy absorption of 1.1 KJ/m^2 at α = 90˚, where the microfibres are perpendicular to the impact direction. Building Bouligand composites with microfibres at α = 90˚, increased impact energy absorption is obtained at a pitch angle of γ = 40˚ with values up to 2.5 KJ/m^2, representing a 140 % increase as compared to the unidirectional composites. Moreover, strong correlation between surface roughness and the energy absorption in Bouligand composites is revealed. The surface roughness could be potentially used to estimate the impact resistance performance of Bouligand composites in the future. From the fracture morphologies, we observed hybrid fracture mechanisms with crack twisting and crack bridging in Bouligand composites during impact in the experiment and in the numerical simulations. As the pitch angle increases, the fracture surface morphologies transitions from crack-twisting–dominated patterns to crack bridging–dominated patterns. In addition to dynamic impact, the flexural strength and modulus of the Bouligand composites at γ = 40˚ also exhibit maximum values of 37 MPa and 2.26 GPa, respectively.

Thanks to the use of DIW as the 3D printing process, the absence of micro-voids, the low porosity and the good interface binding between each deposited filaments prevented macroscopic delamination under impact loading as compared to what has been reported in FDM composites.[6] Furthermore, previous investigations reported that the increase of microfiber loading results in more microfiber slippage and pull-out, enabling increased impact energy absorption.[27] In this work, the microfibers concentration could be prepared higher than 35 wt% in the ink through adjusting the contents of carbon black and CNTs. Therefore, we could improve the impact performance using higher concentration of glass fibres in Bouligand composites according to the practical application. Furthermore, surface modification of glass microfibres using small molecules such as silane coupling agents, to improve the interface compatibility with the matrix is also an option to enhance the performance of the Bouligand composites.[28] As reported by Kaijin et al.,[7] the longer aspect ratio of fibre decreased the critical pitch angle and further enhanced the energy absorption. In our work, the aspect ratio of glass fibres is 2-30, which is shorter than the fibres in the beetle's exoskeleton (aspect ratio at 50).[29] To properly increase the aspect ratio of fibres but avoid the clog at the tip of nozzle, thinner commercial glass fibres or carbon fibres could be employed in the fabrication of Bouligand composites. Moreover, biomaterials such as hydroxyapatite mineral microfibers or SiC whiskers could be introduced in this ink to extend their applications.

To sum up, this unique printing technique allows both microstructure and macro shape design simultaneously to enhance the mechanical properties, in particular the impact resistance, and extend the practical applications of fibre composites in aerospace, the automotive industry, and defence, among others.

Acknowledgements

This research was funded by the National Research Foundation of Singapore, Singapore (Award NRFF12 2020–0002). We acknowledge Peifang Dee for helping with the micro-CT test.

Author contributions

Guan Lizhi: Writing – original draft, Visualization, Investigation, Data curation, Conceptualization. Peng Weixiang– Writing – review & editing, Data curation, Investigation. Rachel Ng Jing Wen Writing – review & editing, Data curation, Investigation. Fan Jingbo: Writing – review & editing, Investigation, Data curation. Le Ferrand Hortense: Writing – review &editing, Conceptualization, Supervision, Funding acquisition.

Data availability

All data are available in this manuscript and in the attached supplementary files. Additional information can be requested to the authors.

Conflict of interest

The authors declare no conflict of interest.

References

1. Le Ferrand, H., Bouville, F., Niebel, T.P. & Studart, A.R. Magnetically assisted slip casting of bioinspired heterogeneous composites. *Nat. Mater.* **14**, 1172-1179 (2015).
2. Patek, S.N. & Caldwell, R.L. Extreme impact and cavitation forces of a biological hammer: strike forces of the peacock mantis shrimp Odontodactylus scyllarus. *J. Exp. Biol.* **208**, 3655-3664 (2005).
3. Weaver, J.C. et al. The Stomatopod Dactyl Club: A Formidable Damage-Tolerant Biological Hammer. *Science* **336**, 1275-1280 (2012).

4. Guarín-Zapata, N., Gomez, J., Yaraghi, N., Kisailus, D. & Zavattieri, P.D. Shear wave filtering in naturally-occurring Bouligand structures. *Acta Biomater.* **23**, 11-20 (2015).
5. Liu, J., Li, S., Fox, K. & Tran, P. 3D concrete printing of bioinspired Bouligand structure: A study on impact resistance. *Addit. Manuf.* **50**, 102544 (2022).
6. Yin, S. et al. Tough Nature-Inspired Helicoidal Composites with Printing-Induced Voids. *Cell Rep. Phys. Sci.* **1**, 100109 (2020).
7. Wu, K. et al. Discontinuous fibrous Bouligand architecture enabling formidable fracture resistance with crack orientation insensitivity. *Proc. Natl. Acad. Sci. U. S. A.* **117**, 15465-15472 (2020).
8. Apichattrabrut, T. & Ravi-Chandar, K. Helicoidal Composites. *Mech. Adv. Mater. Struct.* **13**, 61-76 (2006).
9. Cheng, L., Thomas, A., Glancey, J.L. & Karlsson, A.M. Mechanical behavior of bio-inspired laminated composites. *Compos. - A: Appl. Sci.* **42**, 211-220 (2011).
10. Grunenfelder, L.K. et al. Bio-inspired impact-resistant composites. *Acta Biomater.* **10**, 3997-4008 (2014).
11. Chen, S.-M. et al. Biomimetic twisted plywood structural materials. *Natl. Sci. Rev.* **5**, 703-714 (2018).
12. Luo, Y. et al. Modulating of Bouligand Structure and Chirality Constructed Bionically Based on the Self-Assembly of Chitin Whiskers. *Biomacromolecules* (2023).
13. Yang, Y. et al. Recent Progress in Biomimetic Additive Manufacturing Technology: From Materials to Functional Structures. *Adv. Mater.* **30**, 1706539 (2018).
14. Yang, Y. et al. Biomimetic Anisotropic Reinforcement Architectures by Electrically Assisted Nanocomposite 3D Printing. *Adv. Mater.* **29**, 1605750 (2017).
15. Hausmann, M.K. et al. Dynamics of Cellulose Nanocrystal Alignment during 3D Printing. *ACS Nano* **12**, 6926-6937 (2018).
16. Saadi, M.A.S.R. et al. Direct Ink Writing: A 3D Printing Technology for Diverse Materials. *Adv. Mater.* **34**, 2108855 (2022).
17. Corker, A., Ng, H.C.H., Poole, R.J. & García-Tuñón, E. 3D printing with 2D colloids: designing rheology protocols to predict 'printability' of soft-materials. *Soft Matter* **15**, 1444-1456 (2019).
18. Cantwell, W.J. & Morton, J. The impact resistance of composite materials — a review. *Composites* **22**, 347-362 (1991).
19. Puthanveetil, S., Liu, W.C., Riley, K.S., Arrieta, A.F. & Le Ferrand, H. Programmable multistability for 3D printed reinforced multifunctional composites with reversible shape change. *Compos. Sci. Technol.* **217**, 109097 (2022).
20. Püspöki, Z., Storath, M., Sage, D. & Unser, M. in Focus on Bio-Image Informatics (eds. De Vos, W.H., Munck, S. & Timmermans, J.-P.) 69-93 (Springer International Publishing, Cham, 2016).
21. Sun, L., Gibson, R.F., Gordaninejad, F. & Suhr, J. Energy absorption capability of nanocomposites: A review. *Compos. Sci. Technol.* **69**, 2392-2409 (2009).
22. Guan, L.-Z. et al. Mechanical properties and fracture behaviors of epoxy composites with phase-separation formed liquid rubber and preformed powdered rubber nanoparticles: A comparative study. *Polym. Compos.* **36**, 785-799 (2015).
23. Ding, Y., Zeng, W., Wang, Q. & Zhang, Y. Topographical analysis of fractured surface roughness of macro fiber reinforced concrete and its correlation with flexural toughness. *Constr Build Mater.* **235**, 117466 (2020).
24. Erdem, S. & Blankson, M.A. Fractal–fracture analysis and characterization of impact-fractured surfaces in different types of concrete using digital image analysis and 3D nanomap laser profilometery. *Constr Build Mater.* **40**, 70-76 (2013).
25. Ficker, T. & Martišek, D. Digital fracture surfaces and their roughness analysis: Applications to cement-based materials. *Cem. Concr. Res.* **42**, 827-833 (2012).

26. Yan, X., Reiner, J., Bacca, M., Altintas, Y. & Vaziri, R. A study of energy dissipating mechanisms in orthogonal cutting of UD-CFRP composites. *Compos. Struct.* **220**, 460-472 (2019).
27. H R, M. et al. Effect of Short Glass Fiber Addition on Flexural and Impact Behavior of 3D Printed Polymer Composites. *ACS Omega* **8**, 9212-9220 (2023).
28. Park, S.-J. & Jin, J.-S. Effect of Silane Coupling Agent on Interphase and Performance of Glass Fibers/Unsaturated Polyester Composites. *J. Colloid Interface Sci.* **242**, 174-179 (2001).
29. Yang, R., Zaheri, A., Gao, W., Hayashi, C. & Espinosa, H.D. AFM Identification of Beetle Exocuticle: Bouligand Structure and Nanofiber Anisotropic Elastic Properties. *Adv. Funct. Mater.* **27**, 1603993 (2017).